

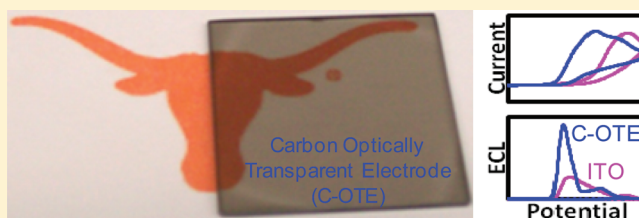
Carbon Optically Transparent Electrodes for Electrogenenerated Chemiluminescence

E. Kate Walker, David A. Vanden Bout,* and Keith J. Stevenson*

Department of Chemistry and Biochemistry, Center for Electrochemistry, Center for Nano- and Molecular Science and Technology, The University of Texas at Austin, Austin, Texas 78712, United States

S Supporting Information

ABSTRACT: This study investigates pyrolyzed photoresist film (PPF)-based carbon optically transparent electrodes (C-OTEs) for use in electrogenerated chemiluminescence (ECL) studies. Oxidative–reductive ECL is obtained with a well-characterized ECL system, C8S3 J-aggregates with 2-(dibutylamino)ethanol (DBAE) as coreactant. Simultaneous cyclic voltammograms (CVs) and ECL transients are obtained for three thicknesses of PPFs and compared to nontransparent glassy carbon (GC) and the conventional transparent electrode indium tin oxide (ITO) in both front face and transmission electrode cell geometries. Despite positive potential shifts in oxidation and ECL peaks, attributed to the internal resistance of the PPFs that result from their nanoscale thickness, the PPFs display similar ECL activity to GC, including the low oxidation potential (LOP) observed for amine coreactants on hydrophobic electrodes. Reductive–oxidative ECL was obtained using the well-studied ECL luminophore Ru(bpy)₃²⁺, where the C-OTEs outperformed ITO because of electrochemical instability of ITO at very negative potentials. The C-OTEs are promising electrodes for ECL applications because they yield higher ECL than ITO in both oxidative–reductive and reductive–oxidative ECL modes, are more stable in alkaline solutions, display a wide potential window of stability, and have tunable transparency for more efficient detection of ECL.



INTRODUCTION

Electrogenated chemiluminescence (ECL) is a “zero background” analytical technique that combines chemiluminescence with the control of electrochemistry to generate reactive species, *in situ*, that can recombine to emit light.^{1–4} ECL has many applications in the development of sensors and biosensors.^{1–3} More recently, ECL imaging has been presented as a platform for single cell analysis,⁵ used to study the corrosion of copper contacts,⁶ and utilized as an imaging technique to study oxidation mechanisms in semiconductor polymer films used for organic light-emitting devices (OLEDs).^{7–10} Both imaging and nonimaging ECL studies can benefit from transparent electrodes because collecting light through the electrode reduces error from specular and diffuse scattering processes and inner filter effects (reabsorption and self-absorption). The transmission cell geometry is also more efficient because it affords an increased collection angle, resulting in more efficient light collection. Recently, Wang et al. demonstrated that transparent electrodes are necessary when ECL emission occurs solely at the electrode interface, such as with their ECL sandwich immunoassay based on quantum dots bound to opaque magnetic beads.¹¹ Much of the ECL literature utilizes bulk opaque electrodes (e.g., platinum, gold, glassy carbon), with considerably fewer reports of ECL on transparent electrodes.^{1–4} The conventional transparent electrode material indium tin oxide (ITO) is not optimal for ECL studies because its hydrophilic surface chemistry generates an overpotential with hydrophobic coreactants and its accessible potential window is not wide

enough for common ECL luminophores.^{1,5,12–15} Therefore, new transparent electrodes with specifically tailored surface chemistry must be explored for the continuing growth of ECL methods and applications.

Recently, new thin film deposition methods have been developed to make and modify transparent electrodes for ECL. Specifically, Zhu et al. reported reductive–oxidative ECL at a transparent (4.5–6% for 375–850 nm) silver nanowire (AgNW) electrode,¹⁶ while Chen et al. reported oxidative–reductive ECL at a transparent (70–90% for 400–800 nm) indium tin oxide (ITO) electrode modified with 4 nm gold nanoparticles (AuNPs) and a fluorosurfactant (FSO).¹⁷ The AgNW electrodes exhibited limited transmittance and were limited to reductive–oxidative ECL since the silver electrode itself would oxidize and dissolve at potentials necessary for oxidative–reductive ECL. The FSO-AuNPs-ITO exhibited a higher transmittance, and the FSO surfactant allowed the typically hydrophilic ITO electrode to access the low oxidation potential (LOP) ECL wave for amine coreactants that is observed on hydrophobic electrodes.^{18–20} Similarly, Huang et al. and Benoist et al. increased oxidative–reductive ECL intensity by modifying ITO with presynthesized ITO nanoparticles (~80% at 610 nm)²¹ and gold-coated TiO₂,²² respectively. Wang et al. observed stronger oxidative–reductive ECL with partially transparent

Received: October 28, 2011

Revised: December 19, 2011

Published: December 21, 2011

Au/CD electrodes versus AuNP modified ITO (no FSO), but there was no data provided about the conductivity or transmittance of the Au/CD electrodes.¹¹ The latter four studies were limited to oxidative–reductive ECL, and all of these synthesis strategies require a lengthy multistep preparation process.

Herein we investigate carbon optically transparent electrodes (C-OTEs) as a more stable and efficient ECL platform. The C-OTEs are generated through pyrolysis of diluted photoresist, generating a pyrolyzed photoresist film (PPF). In a limited context the electrodes have been investigated for use in spectroelectrochemistry and fluorescence imaging applications.^{23–25} Carbon electrodes are desirable for oxidative–reductive ECL since amine-based coreactants (TPrA, DBAE, etc.) display a low oxidation potential on hydrophobic electrodes, such as glassy carbon, which yields intense ECL.^{18–20,26,27} Furthermore, carbon electrodes exhibit wide electrochemical windows of stability in aqueous solution.²⁸ We use C8S3 J-aggregates as a well characterized oxidative–reductive ECL system to assess the C-OTEs versus opaque glassy carbon and transparent ITO electrodes.²⁷ We also demonstrate reductive–oxidative ECL on the C-OTEs using the well-studied ECL luminophore Ru(bpy)₃²⁺. We observe good transmittance (>35% for 190–400 nm, 45–61% for 400–1000 nm) for our thinnest C-OTEs of 11 nm thickness and discuss the effect of this nanoscale thickness on resistance and how it affects the cyclic voltammetry (CV) and ECL responses. The C-OTEs perform favorably versus ITO in both oxidative–reductive and reductive–oxidative ECL studies and are observed to be much more stable in alkaline solutions.

■ EXPERIMENTAL SECTION

Pyrolyzed Photoresist Film Preparation. Pyrolyzed photoresist films (PPFs) were prepared similar to previously reported procedures.^{23,24} Quartz microscope slides, 1 in. square, were purchased from Technical Glass Products and cleaned by heating to 800 °C in air and soaking in piranha (3:1 H₂SO₄:30% H₂O₂) to remove any residual organics. (Caution: piranha is a strong oxidizing solution and must be prepared in a fume hood with proper protection. Always add H₂O₂ to H₂SO₄.) After cleaning, quartz slides were stored in ultrapure H₂O until use. To prepare bulk PPFs, quartz slides were dried with N₂ and taken to the cleanroom. AZ 1518, a positive photoresist, was spin-coated on the quartz at 6000 rpm for 60 s. To prepare transparent PPFs, the AZ 1518 photoresist was diluted with solvent, 1-methoxy-2-propyl acetate (PGMEA), and mixed well prior to spin-coating. Transparent PPFs are identified by their dilution (% v/v). After spin-coating, the photoresist slides were soft baked for 10 min at 90 °C on a hot plate and then transferred to a tube furnace. After purging with 5% H₂: 95% N₂ (~100 mL/min) for 15 min, the photoresist slides were pyrolyzed by heating to 1000 at 5 °C/min and then held at 1000 °C for 1 h before allowing to cool to room temperature slowly. Pyrolyzed films were removed from furnace and stored for 3 days prior to use to allow for the oxide layer to stabilize.²⁹ After characterization, ~150 nm of silver (Kurt J. Lesker, 99.99%) was evaporated (Denton thermal evaporator) on the transparent PPFs (bulk of surface except for active area used for electrochemistry) to minimize contact resistance.²⁴

PPF Characterization. Transmittance spectra of transparent electrodes were acquired with an Agilent Instruments 8453 UV–vis spectrometer with a photodiode array detector. The film thickness and root-mean-square (rms) roughness of the electrodes were measured with a Digital Instruments Nanoscope Dimension 3100 atomic force microscope operated in tapping mode. Scans were collected at 0.5 Hz. An average roughness was calculated from three regions each for three PPFs of each photoresist dilution. The conductivity of the electrodes was determined using a Signatone SP4-62045TRS four-point probe head coupled with an HP3478A multimeter used in the 4-wire Ohms mode. The sheet resistance was calculated using the equation $R_s = C \times V/I$, where C is a correction factor, taken as 0.97 for a thin rectangular

slice ($a/b = 1$), where the length of the sample divided by the probe tip spacing (b/s) is 15.7.³⁰ All measurements were performed on 5–10 electrodes to provide appropriate standard deviation values. Electroactive surface area of the electrodes was measured by chronocoulometry using argon-purged 1 mM hexammineruthenium(III) chloride (Strem Chemicals) in 1 M KNO₃. The potential was stepped from 0 to –0.4 V vs Ag/AgCl (1 M KCl) for 10 s, and the area was calculated from the slope ($m = 2nFAD_0^{1/2}C\pi^{-1/2}$) of the linear portion of the Q vs $t^{1/2}$ plot where $D_0 = 7.3 \times 10^{-6}$ cm² s^{–1}.³¹ Reported electroactive surface area is an average of measurements of at least three of each photoresist dilution. X-ray photoelectron spectroscopy (XPS) was performed with a Kratos Axis DLD spectrometer with an Al K α lamp source. High-resolution spectra of the C 1s (295 to 275 eV) and O 1s (545 to 525 eV) were acquired with a step size of 0.1 eV and a dwell time of 800 ms. Spectra were analyzed using Kratos Vision software with a Shirley background correction. Raman spectra were acquired with a Renishaw inVia microscope using a 514.5 nm argon laser with a 50 \times objective. At least three acquisitions (centered at 1450 cm^{–1}, 40 s integration) were taken of two PPFs of each dilution to observe variations within and between each dilution.

C8S3 J-Aggregate Preparation. The amphiphilic cyanine dye 3,3'-bis(2-sulfopropyl)-5,5',6,6'-tetrachloro-1,1'-diocylbenzimidacarbocyanine (C8S3) was obtained as a sodium salt from FEW Chemicals (Dye S 0440, FEW Chemicals, Germany) and used as received. A 2.92 mM stock solution of C8S3 monomer (MW 902.8 g/mol) was prepared in pure methanol (Spectranalyzed, Fisher Scientific). Self-assembled C8S3 nanotubular J-aggregates were prepared as reported previously.³² Briefly, 130 μ L of the C8S3 stock solution was added to 500 μ L of ultrapure H₂O (>18.2 M Ω cm, Barnstead), agitated, and stored in the dark for 12–24 h before adding a final 500 μ L of H₂O to stabilize the aggregation and result in a final dye concentration of 3.36×10^{-4} M. J-aggregate solutions were used within 2 days of preparation and stored in the dark when not in use. All J-aggregate solution spectra were acquired in a 0.1 mm path length quartz cell (Hellma). Absorbance spectra of J-aggregate solutions were acquired with an Agilent Instruments 8453 UV–vis spectrometer with a photodiode array detector.

Electrochemical Measurements. Electrochemical measurements were performed on J-aggregates immobilized on glassy carbon (GC) plate (1 mm thick, type 2, Alfa Aesar), PPF, or indium tin oxide (ITO)-coated glass electrodes (Delta Technologies, 5–15 Ω). Prior to use, GC plate electrodes were polished with 0.3 μ m alumina, rinsed with H₂O, polished with 0.05 μ m alumina, sonicated for 20 min in H₂O, rinsed with water, and dried with N₂. ITO was cleaned by heating to 80 °C in 30% ethanolamine in water (% v/v) for 20 min, followed by rinsing with methanol and sonicating in ultrapure H₂O for 30 min, and dried with N₂. Films of J-aggregates were prepared by drop-casting 10 μ L of J-aggregate solution on a ~0.5 cm² area of the electrodes followed by drying in the dark for ~2 h. As reported previously, this results in good and reproducible surface coverage, and once dried the J-aggregates remain on the electrode surface when immersed in supporting electrolyte.³² All electrochemical measurements were performed using a home-built cell with a fixed working electrode area of 0.45 cm², path length of 1 cm, cell volume of ~1 mL, a Pt wire counter electrode, and a Ag/AgCl reference electrode (1 M KCl, $E^\circ = +0.236$ V vs NHE, CH Instruments, Austin, TX). All potentials discussed below are versus Ag/AgCl (1 M KCl) unless otherwise denoted. Since most electrochemical reactions examined are irreversible, the potential reported corresponds to maximum anodic current (E_{pa}) as opposed to the usually reported $E_{1/2}$.

Oxidative–reductive electrogenerated chemiluminescence (ECL) was generated with the immobilized C8S3 J-aggregates and the coreactant 2-(dibutylamino)ethanol (DBAE) (MW 173.3 g/mol, density 0.86 g/mL, $pK_a = 9.95$, Fisher Scientific). Previously optimized for maximum ECL signal with C8S3 J-aggregates,²⁷ 17.3 mM DBAE (saturated solution) was dissolved in 1 M KNO₃, and the pH was adjusted with 1 M KOH.^{20,27} ECL scans were from 0 to 1.5 at 0.1 V/s unless otherwise noted. Reductive–oxidative ECL was generated with 3 mM tris (2,2'-bipyridine)dichlororuthenium(II) hexahydrate (Sigma-Aldrich) and 1 mM H₂O₂ as coreactant in 0.15 M phosphate

buffered saline (PBS, pH 7.4), according to previously optimized sample conditions.³³ ECL scans were performed from 0 to -2 at 0.1 V/s.

Simultaneous cyclic voltammograms and ECL were obtained with an Autolab electrochemical workstation (GPES v. 4.9, Eco Chemie, The Netherlands) and a photomultiplier tube (Hamamatsu R4220p), as described elsewhere.³⁴ The photomultiplier tube (PMT) was held at -750 V with a high-voltage power supply (Kepco, Flushing, NY). Photocurrent generated at the PMT was converted to a voltage using an electrometer/high resistance system (model 6517, Keithley, Cleveland, OH) and connected to the Autolab via the analog-to-digital converter (ADC) with external input channel.

RESULTS AND DISCUSSION

Figure 1 compares the percent transmittance of the 33% and 25% PPFs to the conventional transparent electrode indium tin

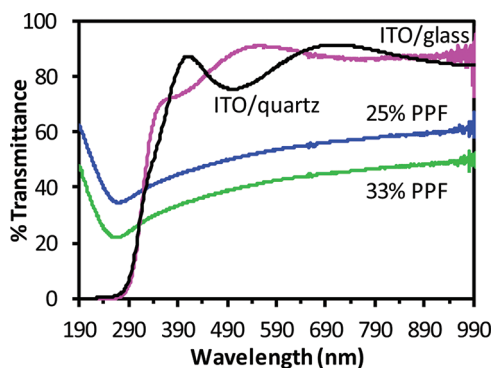


Figure 1. UV-vis-NIR transmittance of 25% (blue) and 33% (green) PPFs versus ITO/glass (pink) and ITO/quartz (black).

oxide-coated (ITO) glass and quartz. The PPFs display a transition at ~ 268 nm due to the $\pi-\pi^*$ transition for electrons delocalized over carbon double bonds, which is consistent with previous studies.²⁴ Although ITO is 20–30% more transparent in the visible range, the PPFs have a clear advantage in the ultraviolet (UV) range with 20–35% more light transmitted than ITO. All ECL experiments were conducted on ITO/glass, but since glass also absorbs in the UV range, a spectrum of ITO/quartz (CEC020Q Präzisions Glas und Optik GmbH, Germany) is included for reference. As reported previously,^{23,24} and displayed in Table 1, the percent transmittance of the PPFs is a function of photoresist dilution, as films cast from more dilute solutions are thinner and can transmit more light. However, as the films decrease in thickness, the sheet resistance of the films increases greatly.²³ Although Schreiber et al. reported 3 nm thick continuous PPFs,³⁵ at 10% (% v/v) photoresist our films were observed to be ~ 6 nm thick and noncontinuous and patchy (data not shown), so 25% was chosen as the most dilute sample in our study. To minimize any contact resistance effects, a film of ~ 150 nm of silver was deposited on the contact area of the transparent PPFs.²⁴ However, the bulk PPFs were conductive enough to use for electrochemical measurements without the silver contact film.

The influence of surface roughness and electroactive surface areas is discussed below.

To determine if the PPF based C-OTEs have a similar ECL performance to glassy carbon (GC) electrodes, simultaneous CV and ECL transients were recorded in a front face geometry at previously optimized ECL conditions for C8S3 J-aggregates.²⁷ Relevant redox equations for this ECL system have been previously reported (Supporting Information).²⁷ The DBAE/C8S3 J-aggregates ECL system was chosen because it has been thoroughly characterized and optimized, and DBAE has recently been presented as a replacement for TPrA as it provides stronger ECL intensity, is less toxic, and is more soluble in aqueous solution.^{11,20,27} Furthermore, C8S3 J-aggregates emit light at the same wavelength (~ 600 nm) as the well studied $\text{Ru}(\text{bpy})_3^{2+}$ luminophore, as well as emitting at a similar potential via the direct coreactant oxidation mechanism. As mentioned earlier, transparent carbon electrodes could be more promising for ECL imaging studies due to the low oxidation potential (LOP) observed for amine coreactants on hydrophobic electrodes (~ 0.6 V) versus that observed on hydrophilic electrodes such as ITO (~ 1.2 V) as well as a wide potential window in both acidic and basic solutions (Supporting Information).^{18,19,26,27} Figure 2 displays

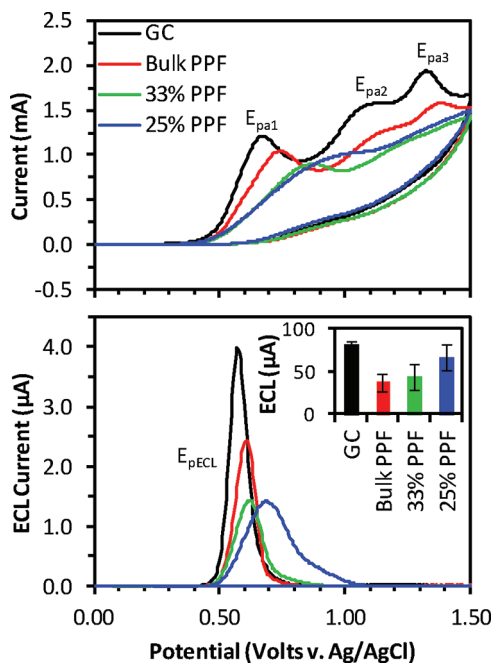


Figure 2. Simultaneous CV (top) and ECL (bottom) transients of immobilized C8S3 J-aggregates with 17.3 mM DBAE in 1 M KNO_3 , pH 12.8. Scan rate is 0.1 V/s. Inset: integrated ECL intensity average for each electrode, with standard deviation represented as error bars.

representative CV and ECL transients, and Table 2 compares the oxidation (E_{pa}) and ECL (E_{PECL}) peak potentials of three thicknesses of PPFs to glassy carbon (GC). The undiluted,

Table 1. Characterization of Transparent and Bulk PPF Electrodes

photoresist dilution (v/v)	%T at 268 nm	%T at 600 nm	film thickness (nm)	R_s (Ω/\square)	rms roughness (nm)	electroactive surface area (cm^2)
25%	35 ± 1	54 ± 1	11 ± 1	1850 ± 70	1.01 ± 0.06	0.70 ± 0.03
33%	22 ± 1	43 ± 1	22 ± 2	1180 ± 40	0.71 ± 0.03	0.73 ± 0.04
100% (bulk)	n/a	n/a	250 ± 20	97 ± 3	0.39 ± 0.07	0.70 ± 0.02

Table 2. CV and ECL Peak Potentials at pH 12.8

electrode material	volts vs Ag/AgCl (1 M KCl)			
	E_{pa1}	E_{pa2}	E_{pa3}	E_{pECL}
GC	0.659 ± 0.005	1.14 ± 0.01	1.318 ± 0.008	0.569 ± 0.003
bulk PPF	0.723 ± 0.005	1.20 ± 0.01	1.38 ± 0.01	0.607 ± 0.003
33% PPF	0.86 ± 0.01			0.64 ± 0.01
25% PPF	1.01 ± 0.02			0.68 ± 0.02

opaque, “bulk” PPFs displayed the same three electrochemical peaks as observed on GC, with a small positive shift (64 mV for peak 1), similar to what has been previously ascribed to a kinetic effect arising from differences in surface chemistry affecting electrochemical systems that depend on surface interactions.²⁹ The first peak (E_{pa1}) corresponds to the oxidation of the 17.3 mM DBAE coreactant,^{20,27} which is dependent on surface interactions (inner-sphere electron transfer), as observed with the large difference in oxidation potentials on ITO versus GC. The second peak (E_{pa2}) is only observed in the presence of DBAE (Supporting Information) and is ascribed to oxidation of a secondary amine produced from the first oxidation of the tertiary amine, a process which has been previously observed for similar tertiary amines and is known to be encouraged by aqueous alkaline conditions such as these.^{36–38} Repetitive cycling studies show a decrease in overall current (Supporting Information) consistent with previous reports of surface modification of glassy carbon electrodes by the amine radicals produced during oxidation.^{36–38} However, it should be noted that for this ECL system most light is emitted by ~ 1 V, so limiting the potential range to this will result in slower electrode modification and passivation (Supporting Information). The third peak (E_{pa3}) corresponds to the oxidation of residual methanol contained within the J-aggregate double-walled tubular structure (Supporting Information).³⁹ The oxidation of the C8S3 J-aggregates is not observed, as it is convoluted with the first peak corresponding to the DBAE coreactant.²⁷ Similarly, the ECL transient retains the same sharpness of peak as GC, but with a slight positive shift (37 mV). Both the CV and ECL response of the bulk PPF show that it displays the same electrochemical and ECL behavior as GC, although slightly diminished. While the thinner films (33%, 25% PPF) display a similar first oxidation peak corresponding to the 17.3 mM DBAE coreactant, an increasing positive shift in the potential of the peak is observed for each subsequent photoresist dilution, and the second and third oxidation peaks become hard to resolve. Similarly, the ECL peak shifts more positive with increasing photoresist dilution and broadens. Interestingly, this positive shift is not detrimental to the ECL output as integration of the ECL peaks (inset) shows that there are a larger number of total integrated photon counts from the 25% PPF electrode than the 33% or bulk PPF electrodes. As this positive shift in potential and change in ECL profile could be due to surface effects such as roughness or chemical functionality,⁴⁰ or the internal resistance of the electrode,^{29,41} we performed follow-up experiments to determine the influence of these parameters.

As shown in Table 1, the surface roughness increases as with photoresist dilution. This is consistent with previous reports²³ and is attributed to the roughness of the underlying quartz. However, this small difference in roughness does not have a significant or direct effect on the electrochemistry as all three thicknesses of PPFs were determined to have the same

electroactive surface area versus each other as well as versus glassy carbon (0.66 ± 0.07 nm). Instead, the increase in surface roughness might yield different surface functional groups due to an increase in the number of dangling bonds or edge plane sites. Recently, Chiu et al. demonstrated that increasing the C–OH to C–C ratio of carbon electrode surfaces by pre-anodization in acidic or basic solution can lead to differences in CV and ECL transients and ultimately increased ECL.⁴⁰ Figure 3

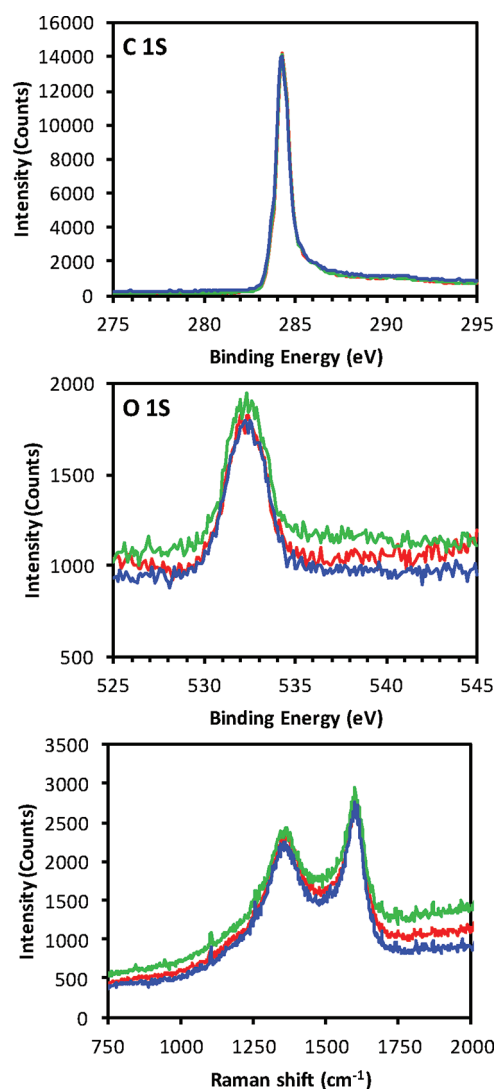


Figure 3. XPS and Raman spectra of bulk PPF (red), 33% PPF (green), and 25% PPF (blue).

displays the X-ray photoelectron spectra of the carbon 1s (C 1s) and oxygen 1s (O 1s) orbitals, which would display any differences in chemical functionalization of the surface. Both the C 1s and O 1s spectra show that the surface functional groups are the same, regardless of photoresist dilution and therefore film thickness or roughness. Figure 3 also compares the Raman spectra of the D band (~ 1350 cm^{-1} , disordered) and G band (~ 1600 cm^{-1} , graphitic) of all three PPF thicknesses.²⁸ Again, the peaks are observed to be maintained across all thicknesses of PPFs. Furthermore, the D/G intensity ratio is calculated to be 0.8, which corresponds to an average crystallite size of 55 Å,⁴² which is similar to the 28 Å previously determined for bulk PPFs via X-ray line broadening.⁴³

A high internal resistance would cause a large potential drop across the electrode surface, and the resulting electrochemical data would show a positive potential shift (overpotential) with increasing resistance, similar to the effect we observe in Figure 2.^{29,41} To determine if our observations are a function of ohmic potential drop due to the internal resistance, we performed the same ECL measurements on the 25% and 33% PPFs at a scan rate of 10 mV/s instead of 100 mV/s, where the slower scan rate would decrease the current and therefore the ohmic (iR) error, resulting in less of an overpotential for the electrochemical processes.⁴¹ Figure 4 shows that slowing the scan rate

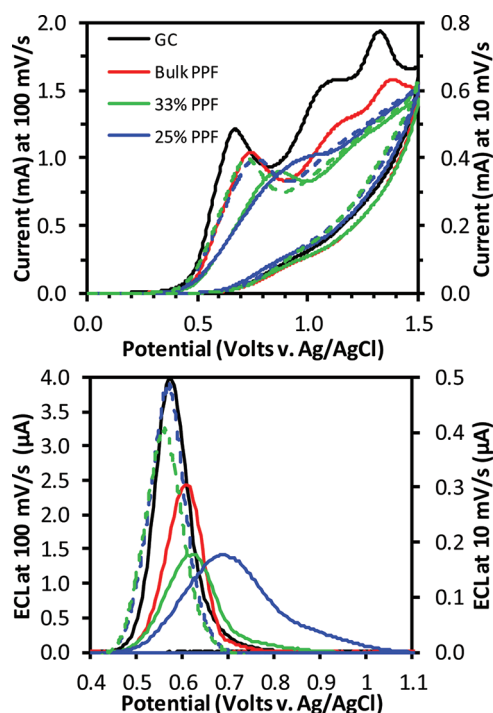


Figure 4. Simultaneous CV (top) and ECL (bottom) transients obtained at 100 mV/s (solid lines) and 10 mV/s (dashed lines) on GC and PPF electrodes. Sample was immobilized C8S3 J-aggregates with 17.3 mM DBAE in 1 M KNO_3 , pH 12.8. Potential range for ECL transients is displayed from 0.4 to 1.1 V for emphasis.

from 100 to 10 mV/s causes the DBAE oxidation peak to move to a less positive potential, concurrent with that of the bulk PPF. Furthermore, the ECL transients shift less positive and narrow to a sharper peak, concurrent with the potential and peak shape observed for ECL on glassy carbon at 100 mV/s. Therefore, the increased potential and broadening of the ECL peak upon increasing photoresist dilution are attributed to an ohmic potential drop from the high internal resistance of the electrode. Because of the potential drop across the electrode, it takes longer for all of the C8S3 molecules to oxidize, allowing more DBAE radicals to reach the C8S3 molecules before they oxidize irreversibly,³² which results in a slower emission of photons from the sample as discussed above (Figure 2, inset).

To further evaluate these transparent carbon electrodes, we compared them to the conventional transparent indium tin oxide (ITO) electrode. However, we were unable to compare these electrode materials at the previously optimized pH of 12.8 ± 0.1 since the ITO reacts in strong base and begins dissolution at this high pH (Supporting Information). Instead, we compared GC, all three PPFs, ITO, and fluorine tin oxide

(FTO) in a front face geometry at $\text{pH } 10.8 \pm 0.1$ (Supporting Information). All of the carbon electrodes displayed the low oxidation potential (LOP) observed for amine coreactants on hydrophobic electrodes, whereas both ITO and FTO displayed the coreactant oxidation potential at ~ 0.6 V more positive.^{18,19} As a result, the carbon-based electrodes produce a narrower, sharper emission at a lower potential.

To best understand the interplay between electrode transparency and chemical composition of the surface, we compared the C-OTEs versus ITO in a through the electrode transmission cell geometry at $\text{pH } 10.8 \pm 0.1$ (Figure 5). Again, the

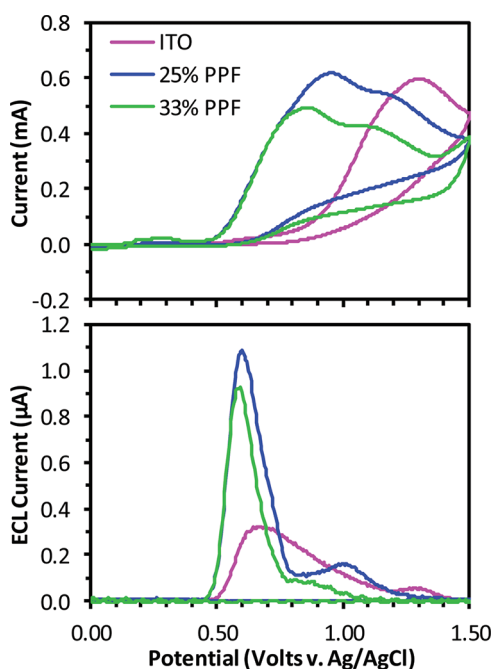


Figure 5. Simultaneous CV (bottom) and ECL (top) transients of C8S3 J-aggregates immobilized on electrodes with 17.3 mM DBAE in 1 M KNO_3 , pH 10.8. ECL was collected through the ITO (pink), 33% PPF (green), and 25% PPF (blue) electrodes. Scan rate was 0.1 V/s.

carbon electrodes are observed to have a sharper emission profile at a lower potential. Even though the percent transmittance of ITO is much higher than the C-OTEs, the 33% PPF ($27 \pm 5 \mu\text{A}$) results in approximately the same amount of ECL detected as ITO ($28 \pm 2 \mu\text{A}$), whereas the 25% PPF ($41 \pm 11 \mu\text{A}$) results in more ECL detected. This illustrates that percent transmittance is not the sole concern when it comes to transparent electrodes for ECL and that it is very important to understand how the surface chemistry can affect the electrochemical transients. Clearly, the C-OTEs yield better signal for oxidative–reductive ECL experiments that rely on an amine-based coreactant (e.g., DBAE, TPRA). It is interesting to note that the ECL shoulder at higher potentials on the PPF electrodes could be due to the oxidation of the secondary amine generated *in situ* by the process discussed above.

In addition, the transparency of these carbon electrodes allowed us to perform transmission spectroelectrochemistry to elucidate the origin of an emission difference previously observed between fluorescence and ECL of the C8S3 J-aggregates. C8S3 J-aggregates are double-walled nanotubular structures (diameter = 13 nm) that are comprised of self-assembled amphiphilic cyanine dyes. The supramolecular

structure causes packing of the dye molecules that allows for coupling of the transition dipoles, resulting in a highly efficient delocalized exciton in the form of two narrow optical transitions (590 and 600 nm) with no Stokes shift between absorption and emission. In our previous work, we obtained an ECL spectrum of the C8S3 J-aggregates that displayed a slight merging and offset of the emission (~ 595 nm) from immobilized aggregates on GC versus the solution fluorescence and film on glass fluorescence (590 and 600 nm).²⁷ These differences were attributed to the surface chemistry of the carbon electrode affecting the supramolecular structure of the C8S3 J-aggregates upon immobilization, since previous spectroelectrochemical studies on ITO in 1 M KNO_3 (pH 5.78) showed the two peaks retained in the absorption spectrum.³² However, because GC is opaque, we were unable to pursue further transmission spectroelectrochemical studies to pinpoint the true cause from the three main possibilities of differences in surface chemistry between electrodes, presence/absence of the DBAE coreactant, or the high pH for optimal ECL. Figure 6 displays

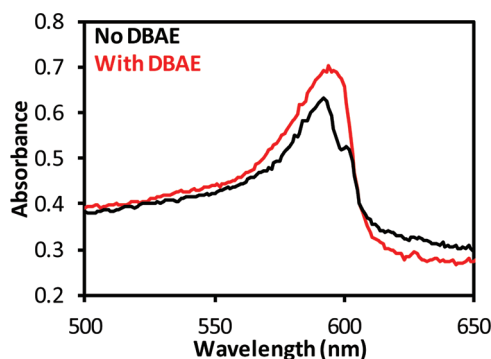


Figure 6. Representative UV-vis spectra of C8S3 J-aggregates (top) immobilized on 33% PPF electrodes in the presence (red) and absence (black) of 17.3 mM DBAE coreactant.

absorption spectra for immobilized aggregates in the presence and absence of DBAE. The control, at the same pH but with no DBAE, shows both absorption peaks at the expected wavelengths (591 ± 1 and 601 ± 1 nm), just as was observed previously on ITO at neutral to acidic pH. Therefore, it is neither the difference in pH nor the difference in electrode that causes the spectral changes. In the presence of DBAE, the two peaks merge and the maximum wavelength (594 ± 1 nm) shifts to what was previously observed for the ECL spectrum (~ 595 nm). Therefore, the DBAE coreactant is the primary cause for changes in spectra. This is most likely due to the amphiphilic DBAE molecule being able to partition into the C8S3 supramolecular structure and altering the transition dipole coupling between aggregates.³⁹

Finally, we assessed the C-OTEs for reductive-oxidative ECL with the well-studied ECL luminophore $\text{Ru}(\text{bpy})_3^{2+}$.³³ Figure 7 displays CV and ECL transients for ECL of $\text{Ru}(\text{bpy})_3^{2+}$ in the presence of the coreactant H_2O_2 on GC, 33% PPF, and ITO. Data were also acquired in the transmission through the electrode cell geometry (Supporting Information). On GC we observe the first reduction peak (-0.65 V) of H_2O_2 , followed by the reduction of $\text{Ru}(\text{bpy})_3^{2+}$ in two forms, a prewave (-1.45 V) due to adsorbed $\text{Ru}(\text{bpy})_3^{2+}$ and then a diffusion-controlled wave (-1.52 V) for $\text{Ru}(\text{bpy})_3^{2+}$.³³ The return oxidation scan shows a sharp oxidation peak (-1.33 V) associated with stripping of adsorbed and precipitated $\text{Ru}(\text{bpy})_3^{2+}$ as it is oxidized to $\text{Ru}(\text{bpy})_3^{3+}$ and becomes more soluble in the aqueous solution. The 33% PPF CV

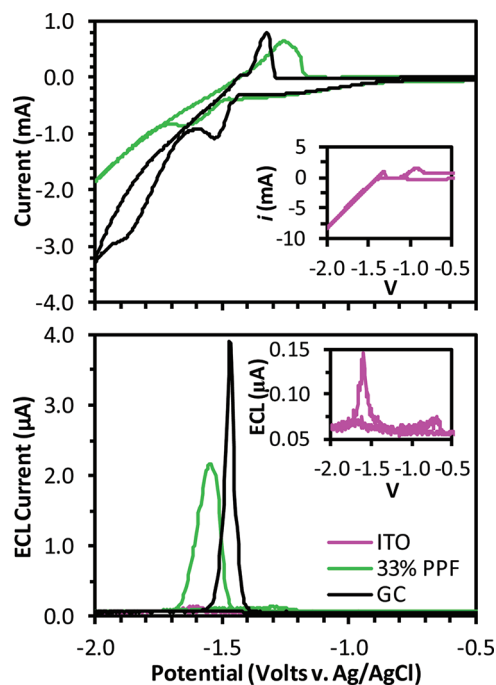


Figure 7. Simultaneous CV (top) and ECL (bottom) transients of 3 mM $\text{Ru}(\text{bpy})_3^{2+}$ with 1 mM H_2O_2 in 0.15 M PBS, pH 7.4 on GC, ITO, and 33% PPF electrodes. Scan from 0 to -2 V at 0.1 V/s. Inset displays ITO transient.

shows similar features to GC with a similar peak for H_2O_2 reduction (-0.67 V) and the peak of the prewave of $\text{Ru}(\text{bpy})_3^{2+}$ reduction (-1.45 V). However, the diffusion controlled wave is at a slightly more negative potential and is broader (-1.67 V), and on the reverse oxidation scan, the stripping peak is observed at slightly more positive potentials (-1.25 V) and has broadened, a result of the internal resistance effects discussed above. The ECL peaks on GC (-1.47 V) and 33% PPF (-1.55 V) are again similar except for the peak broadening and potential shift due to the internal resistance of the PPF electrode, with the 33% PPF yielding more photons emitted upon integration of the ECL peak. On ITO we observe very different behavior in both the CV and ECL transients. The reduction of H_2O_2 (-0.66 V) is observed, but at -1.4 V we observe the onset of a linear increase in current with potential, and there is an additional oxidation (-0.93 V) on the reverse scan, and very little ECL is detected. Upon examination the previously transparent ITO electrode has formed an opaque film on the electrode surface. This change in the chemical composition of the electrode upon cathodic cycling has been studied in depth previously and is attributed to segregation of indium on the surface of the ITO from either diffusion or preferential dissolution of tin from the film.¹² Therefore, the C-OTEs have a distinct advantage over ITO for reduction-oxidation ECL studies.

CONCLUSIONS

We have reported both oxidative-reductive and reductive-oxidative ECL studies using carbon optically transparent electrodes (C-OTEs) based on pyrolyzed photoresist films (PPFs). Three dilutions of photoresist were used to create PPFs of varying thickness and percent transmittance, with the most dilute solution (25%) yielding films 11 nm thick with 54% transmittance at 600 nm. XPS and Raman showed that the surface chemistry was consistent across all three photoresist dilutions. Although we observed small differences in surface

roughness, this did not affect the electroactive surface area. Sheet resistance increased with dilution and decreasing film thickness, which caused potential shifts and peak broadening in the CV and ECL transients versus glassy carbon electrodes. The C-OTEs yielded higher ECL than the traditional transparent electrode, ITO, in both oxidative–reductive and reductive–oxidative studies, with the former due to the low oxidation potential for amine coreactants on carbon electrodes and the latter due to electrochemical instability of the ITO at very negative potentials. The transparency of the C-OTEs was also utilized for a transmission UV–vis spectroelectrochemical study.

Overall, PPF-based C-OTEs are very promising for both anodic and cathodic ECL studies because of their surface chemistry, wide electrochemical potential window of stability, and tunable optical transparency across the UV–vis range.

■ ASSOCIATED CONTENT

■ Supporting Information

C8S3 J-aggregates ECE oxidation scheme, ECL mechanisms, background scans of 25% PPF in acidic and alkaline solutions, identification of oxidation peaks by CV comparison, discussion of amine oxidation and effects of electrode cycling, electrochemical instability of ITO in high pH coreactant solutions, comparison of ECL at electrodes (GC, PPFs, ITO, FTO) in front face geometry at pH 10.8, and ECL of Ru(bpy)₃²⁺ obtained in transmission cell geometry. This material is available free of charge via the Internet at <http://pubs.acs.org>.

■ AUTHOR INFORMATION

Corresponding Author

*E-mail: davandenbout@mail.utexas.edu (D.A.V.B.); Steven@cm.utexas.edu (K.J.S.).

■ ACKNOWLEDGMENTS

Financial support for this work was provided by the R.A. Welch Foundation (Grant F-1529) and the National Science Foundation (CHE-1012790). We thank Dr. Allen Bard for the use of the Autolab/PMT setup for ECL measurements and Jacob Goran for assistance with the XPS measurements. We thank the National Science Foundation (CHE-0618242) for funding the X-ray Photoelectron Spectrometer used in this work.

■ REFERENCES

- (1) Hu, L.; Xu, G. *Chem. Soc. Rev.* **2010**, *39*, 3275–3304.
- (2) Forster, R. J.; Bertocello, P.; Keyes, T. E. *Annu. Rev. Anal. Chem.* **2009**, *2*, 359–385.
- (3) Miao, W. *Chem. Rev.* **2008**, *108*, 2506–2553.
- (4) Richter, M. M. *Chem. Rev.* **2004**, *104*, 3003–3036.
- (5) Dolci, L. S.; Zamarini, S.; Ciana, L. D.; Paolucci, F.; Roda, A. *Anal. Chem.* **2009**, *81*, 6234–6241.
- (6) McMurray, H. N.; Barrett, Z. *ECS Trans.* **2007**, *3*, 219–226.
- (7) Chen, J.-T.; Chang, Y.-L.; Guo, S.; Fabian, O.; Lackowski, W. M.; Barbara, P. F. *Macromol. Rapid Commun.* **2011**, *32*, 598–603.
- (8) Chen, J.-T.; Chang, Y.-L.; Fabian, O.; Guo, S.; Lackowski, W. M.; Barbara, P. F. *J. Phys. Chem. C* **2011**, *115*, 10256–10263.
- (9) Guo, S.; Fabian, O.; Chang, Y.-L.; Chen, J.-T.; Lackowski, W. M.; Barbara, P. F. *J. Am. Chem. Soc.* **2011**, *133*, 11994–12000.
- (10) Chang, Y.-L.; Palacios, R. E.; Chen, J.-T.; Stevenson, K. J.; Guo, S.; Lackowski, W. M.; Barbara, P. F. *J. Am. Chem. Soc.* **2009**, *131*, 14166–14167.
- (11) Wang, S.; Harris, E.; Shi, J.; Chen, A.; Parajuli, S.; Jing, X.; Miao, W. *Phys. Chem. Chem. Phys.* **2010**, *12*, 10073–10080.
- (12) Senthilkumar, M.; Mathiyarasu, J.; Joseph, J.; Phani, K. L. N.; Yegnamaran, V. *Mater. Chem. Phys.* **2008**, *108*, 403–407.
- (13) Stotter, J.; Show, Y.; Wang, S.; Swain, G. *Chem. Mater.* **2005**, *17*, 4880–4888.
- (14) Kraft, A.; Hennig, H.; Herbst, A.; Heckner, K.-H. *J. Electroanal. Chem.* **1994**, *365*, 191–196.
- (15) Wilson, R.; Akhavan-Tafii, H.; DeSilva, R.; Schaap, A. P. *Electroanalysis* **2001**, *13*, 1083–1092.
- (16) Zhu, Y.; Hill, C. M.; Pan, S. *Langmuir* **2011**, *27*, 3121–3127.
- (17) Chen, Z.; Zu, Y. *Langmuir* **2007**, *23*, 11387–11390.
- (18) Li, F.; Zu, Y. *Anal. Chem.* **2004**, *76*, 1768–1772.
- (19) Zu, Y.; Bard, A. J. *Anal. Chem.* **2000**, *72*, 3223–3232.
- (20) Liu, X.; Shi, L.; Niu, W.; Li, H.; Xu, G. *Angew. Chem., Int. Ed.* **2007**, *46*, 421–424.
- (21) Huang, R.; Wei, M.-Y.; Guo, L.-H. *J. Electroanal. Chem.* **2011**, *656*, 136–139.
- (22) Benoist, D. M.; Pan, S. *J. Phys. Chem. C* **2010**, *114*, 1815–1821.
- (23) Donner, S.; Li, H.-W.; Yeung, E. S.; Porter, M. D. *Anal. Chem.* **2006**, *78*, 2816–2822.
- (24) Tian, H.; Bergren, A. J.; McCreery, R. L. *Appl. Spectrosc.* **2007**, *61*, 1246–1253.
- (25) Dai, Y.; Swain, G.; Porter, M. D.; Zak, J. *Anal. Chem.* **2008**, *80*, 14–22.
- (26) Zu, Y.; Bard, A. J. *Anal. Chem.* **2001**, *73*, 3960–3964.
- (27) Walker, E. K.; Vanden Bout, D. A.; Stevenson, K. J. *J. Phys. Chem. C* **2011**, *115*, 2470–2475.
- (28) McCreery, R. L. *Chem. Rev.* **2008**, *108*, 2646–2687.
- (29) Ranganathan, S.; McCreery, R. L. *Anal. Chem.* **2001**, *73*, 893–900.
- (30) *Geometric Factors in Four Point Resistivity Measurements*; Haldor Topsoe Semiconductor Division: Haldor Topsoe, Denmark, 1968.
- (31) Wiggins-Camacho, J. D.; Stevenson, K. J. *J. Phys. Chem. C* **2009**, *113*, 19082–19090.
- (32) Lyon, J. L.; Eisele, D. M.; Kirstein, S.; Rabe, J. P.; Vanden Bout, D. A.; Stevenson, K. J. *J. Phys. Chem. C* **2008**, *112*, 1260–1268.
- (33) Choi, J.-P.; Bard, A. J. *Anal. Chim. Acta* **2005**, *541*, 141–150.
- (34) Omer, K. M.; Bard, A. J. *J. Phys. Chem. C* **2009**, *113*, 11575–11578.
- (35) Schreiber, M.; Lutz, T.; Keeley, G. P.; Kumar, S.; Boese, M.; Krishnamurthy, S.; Duesberg, G. S. *Appl. Surf. Sci.* **2010**, *256*, 6186–6190.
- (36) Masui, M.; Sayo, H.; Tsuda, Y. *J. Chem. Soc., B* **1968**, 973–976.
- (37) Deinhammer, R. S.; Ho, M.; Anderegg, J. W.; Porter, M. D. *Langmuir* **1994**, *10*, 1306–1313.
- (38) Adenier, A.; Chehimi, M. M.; Gallardo, I.; Pinson, J.; Vila, N. *Langmuir* **2004**, *20*, 8243–8253.
- (39) von Berlepsch, H.; Kirstein, S.; Hania, R.; Pugzlys, A.; Bottcher, C. *J. Phys. Chem. B* **2007**, *111*, 1701–1711.
- (40) Chiu, M.-H.; Wei, W.-C.; Zen, J.-M. *Electrochem. Commun.* **2011**, *13*, 605–607.
- (41) Ranganathan, S.; McCreery, R.; Majji, S. M.; Madou, M. *J. Electrochem. Soc.* **2000**, *147*, 277–282.
- (42) Knight, D. S.; White, W. B. *J. Mater. Res.* **1989**, *4*, 385–393.
- (43) Kim, J.; Song, X.; Kinoshita, K.; Madou, M.; White, R. *J. Electrochem. Soc.* **1998**, *145*, 2314–2319.